IOP Publishing Nanotechnology

Nanotechnology 32 (2021) 335701 (9pp)

https://doi.org/10.1088/1361-6528/abff8f

Atmospheric-pressure CVD growth of twodimensional 2H- and 1T'-MoTe₂ films with high-performance SERS activity

Bikram Adhikari¹, Tej B Limbu¹, Kizhanipuram Vinodgopal and Fei Yan^{*} ©

Department of Chemistry and Biochemistry, North Carolina Central University, Durham, NC 27707, United States of America

E-mail: fyan@nccu.edu and tejblimbu@gmail.com

Received 6 March 2021, revised 2 May 2021 Accepted for publication 10 May 2021 Published 24 May 2021



Abstract

Two-dimensional (2D) molybdenum ditelluride ($MoTe_2$) is a member of the transition-metal dichalcogenides family, which is an especially promising platform for surface-enhanced Raman scattering (SERS) applications, due to its excellent electronic properties. However, the synthesis of large-area highly crystalline 2D $MoTe_2$ with controllable polymorphism is a huge challenge due to the small free energy difference (\sim 40 meV per unit cell) between semiconducting $2H-MoTe_2$ and semi-metallic 1 $T'-MoTe_2$. Herein, we report an optimized route for the synthesis of 2H- and 1 $T'-MoTe_2$ films by atmospheric-pressure chemical vapor deposition. The SERS study of the as-grown $MoTe_2$ films was carried out using methylene blue (MB) as a probe molecule. The Raman enhancement factor on 1 $T'-MoTe_2$ was found to be three times higher than that on $2H-MoTe_2$ and the 1 $T'-MoTe_2$ film is an efficient Raman-enhancing substrate that can be used to detect MB at nanomolar concentrations. Our study also imparts knowledge on the significance of a suitable combination of laser excitation wavelength and molecule-material platform for achieving ultrasensitive SERS-based chemical detection.

Supplementary material for this article is available online

Keywords: chemical vapor deposition, transition-metal dichalcogenides, phase change material, SERS

(Some figures may appear in colour only in the online journal)

Abbreviation	ns	EM	electromagnetic mechanism	
2D	two-dimensional	FWHM	full width at half maximum	
AFM	atomic force microscopy	НОМО	highest occupied molecular orbital	
APCVD	atmospheric pressure chemical vapor	LOD	limit of detection	
	deposition	LPCVD	low-pressure chemical vapor deposition	
CB	conduction band	LUMO	lowest unoccupied molecular orbital	
CM	chemical mechanism	MB	methylene blue molecular beam epitaxy metal-organic chemical deposition	
CT	charge transfer	MBE		
EF	enhancement factor	MOCVD		
1 These authors	have contributed equally to the work.	MoO_3	molybdenum trioxide	
	m any correspondence should be addressed.	$MoTe_2$	molybdenum ditelluride	

PICT photo-induced charge transfer

PLD pulsed laser deposition PVD physical vapor deposition

SERS surface-enhanced Raman scattering

Te tellurium

TST transition state theory

VB valence band

1. Introduction

Two-dimensional transition metal dichalcogenides (TMDs) have been drawing the attention of the scientific community due to their unique structure and properties. Because of their amazing physical and chemical properties, they are potential candidates for chemical and biological sensors [1], electronics [2], optoelectronics [3], catalysts [4], supercapacitors, and energy storage [5]. Among various TMDs, MoTe₂ is a fascinating layered material that commonly exists in three crystalline forms: hexagonal α (2H-MoTe₂), monoclinic β (1 T'-MoTe₂), and orthorhombic β' (1T-MoTe₂) [6]. However, only 2H-MoTe₂ and 1 T'-MoTe₂ are thermodynamically stable and have been prepared in laboratories and are being explored [7]. 2H-MoTe₂ is semiconducting with a layerdependent bandgap, the bulk of which has an indirect bandgap of 0.88 eV while a monolayer has a direct bandgap around 1.0 eV [8]. Because of its similar bandgap size and higher electron mobility [9], monolayer MoTe₂ stands out as a promising candidate to replace silicon in future electronic and optoelectronic devices. On the other hand, 1 T'-MoTe₂ is semi-metallic and exhibits high charge carrier mobility with a high electron density of states at the Fermi level [8, 10] making it a suitable material for several applications [11]. One of the challenges in synthesizing 2D MoTe₂ is the low reactivity of Mo and Te because of the small electronegativity difference (0.3 eV) between Te and Mo, resulting in the small binding energy for Mo-Te [12, 13]. Furthermore, large-scale and perfect stoichiometric MoTe₂ synthesis with a defined phase is difficult as compared with other TMDs because of the temperature-dependent polymorphism observed in MoTe₂ [14]. Such difficulties associated with the synthesis of 2D MoTe₂ pose significant challenges in bringing these materials into real applications. Hence, there is an urgent need to develop a facile approach for the controlled synthesis of semiconducting and semi-metallic polymorphs of 2D MoTe₂.

SERS is a powerful and sensitive analytical tool that is widely applicable to the molecular-level analysis of chemical and biomolecules [15, 16]. SERS not only provides high sensitivity and the ability to provide a specific 'fingerprint,' but also is non-destructive, capable of real-time operation, and allows *in situ* remote sensing [17]. The Raman signal intensity of any given molecules could be increased because of localized surface plasmon, and/or their physicochemical interaction with the substrate. SERS based on surface plasmon resonance also known as the EM, is effective but poses

several drawbacks such as high fluorescence background and unnecessary catalytic processes facilitated by metal nanostructures [18]. Many studies have shown that 2D materials such as TMDs (e.g. MoS₂, MoSe₂, WSe₂, and NbS₂) are excellent materials for SERS substrates due to their exceptional electronic structure and response to light photons [19-21]. These materials have been proposed to enhance Raman signal by CT interaction between the material and probe molecules, which is known as the CM [22]. Because of its high charge carrier mobility and higher electronic density of states at the Fermi level [8, 10], 1 T'-MoTe₂ is expected to be a better SERS substrate than other 2D materials [23]. To date, several studies have reported that 1 T'-MoTe2 could enhance Raman signal by 6-8 orders of magnitude [24, 25]. However, these reports have explored the SERS properties of either exfoliated or chemical-vapor-deposited 1 T'-MoTe₂, and none of them have explored SERS properties of 2H-MoTe₂. Furthermore, the Raman EF of 2D materials is strongly dependent on the excitation laser wavelength [26, 27] and hence a suitable choice of laser wavelength is required to be made to achieve optimal performance.

PVD such as PLD [28] and MBE [29], and chemical vapor deposition (CVD) technologies such as LPCVD [8, 23], MOCVD [30], and APCVD [31] have been employed to synthesize various 2D materials. However, PVD techniques require a sophisticated pump system for creating ultralow pressure. Furthermore, the domain size of the PVD-grown films is comparatively smaller than those of CVD-grown films, and PVD-grown samples are frequently found to show antisite defects, which are detrimental for optoelectronic applications [32]. Both LPCVD and MOCVD are suitable for growing high-quality and large-area 2D films at low cost, but LPCVD requires a pump and pressure controller system making the setup complicated, and MOCVD requires an additional system to controllably convert solid or liquid precursor to gaseous precursor. Unlike such technologies, APCVD is a simple and cost-effective technique, and the process can be performed at ambient pressure, making it suitable for industrial scale-up production of materials at a lower cost.

Herein, we demonstrate a facile synthesis of 2D MoTe₂ with controllable polymorphism by APCVD. Our approach can be further improved for large-scale synthesis of high-quality 2H- and 1 T'-MoTe₂, and the methodology can also be applied for the controllable growth of other TMD materials. We examined both MoTe₂ polymorphs for their SERS properties by using MB as a probe molecule and compared the SERS efficiency of 2H- and 1 T'-MoTe₂ films using 532 nm and 633 nm excitation sources. The study shows an excellent SERS activity of 2D MoTe₂ film with a Raman EF on the order of 10⁷–10⁸, and a LOD as low as 10 nM for MB.

2. Experimental detail

2.1. Synthesis of 2D MoTe₂ films by APCVD

The phase-controlled synthesis of 2H-MoTe₂ and the 1 T'-MoTe₂ film was carried out using CVD (OTF- 1200X,

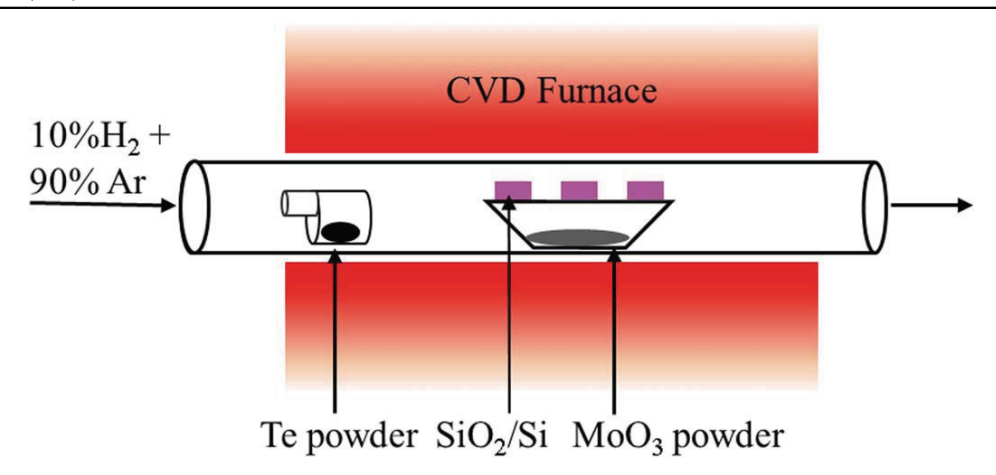


Figure 1. Schematic diagram of a typical APCVD synthesis system.

MTI corporation) under ambient pressure conditions. To synthesize the 2D MoTe₂ films, 5 mg of MoO₃ powder (STREM chemicals Inc.) mixed with 2% NaCl was dispersed in a quartz boat (7 cm length, 1.5 cm height) with the help of a few drops of isopropanol. 300 mg of Te powder (Fisher Scientific) was placed upstream in a small neck container (1.6 cm base diameter, 2.0 cm length, and 0.5 cm neck length) at 10 cm upstream from the edge of the furnace inside the quartz tube (length 79 cm, internal diameter 3.2 cm, and external diameter 3.8 cm) Such a small neck container helps to control the vigorous evaporation of Te when it reaches the maximum temperature. Also, the Te containing neck container was placed in the tube with its neck facing upstream, which helps to spread the gaseous Te coming out of it to the entire volume of the quartz tube (see figure S2 in the supporting file). SiO₂/Si substrates used for the material growth were placed upside down on the quartz boat. The carrier gas (a mixture of $10\% H_2 + 90\% Ar$) flowed throughout the process at the rate of 40 sccm. The growth temperature for 2H- and 1 T'-MoTe₂ films were 650 and 730 °C, respectively, and film deposition time was set at 15 min. The temperatures of the region where Te powder was placed, were \sim 420 °C and \sim 450 °C for the set growth temperatures of 650 and 730 °C for the growth of 2H- and 1 T'-phases, respectively. The temperatures of the furnace were increased at the rate of 25 °C min⁻¹ up to 400 °C and 10 °C min⁻¹ up to 650 °C for 2H-MoTe₂ and at 20 °C min⁻¹ up to 730 °C for 1 T'-MoTe₂ The cooling rates from the growth temperature to 300 °C were set at 15 °C min⁻¹ and 5 °C min⁻¹, respectively, for 2H- and 1 T'- polymorphs, and the furnace was opened to allow further cooling under ambient conditions.

2.2. Characterization using Raman and AFM spectroscopy

A combined RAMAN Microscope-Smart SPM atomic force microscope (LabRAm HR Evolution, Horiba Scientific) was used for the characterization of as-grown 2D MoTe₂ films. The Raman measurements were carried out with a 532 nm excitation laser (0.27 mW laser power, and 20 s exposure time), using 1,800 g mm⁻¹ grating and 100× objective lens.

The thickness of the MoTe₂ films was measured using tapping mode AFM.

2.3. SERS measurements

SERS measurements of as-grown 2D MoTe₂ films were performed using MB as a probe molecule. MB (Fisher Scientific) solution of different concentrations in water was prepared and about $10~\mu l$ of as-prepared MB solution of each concentration starting from the lowest was dropped on the MoTe₂. SERS measurements were performed using LabRAM HR Evolution Raman spectrophotometer of laser intensity 532 nm (0.27 mW power) and 633 nm (0.25 power) for 20 s using a 300 grating mm⁻¹ and $100 \times$ objective lens.

3. Results and discussion

3.1. Synthesis and characterization of 2D MoTe₂ films

Figure 1 shows the schematic for growing 2D MoTe₂ films on SiO₂/Si substrates. Two different strategies were used for the synthesis of these two MoTe₂ polymorphs. At a lower growth temperature, 650 °C, 2H-MoTe₂ films, and at a relatively higher temperature, 730 °C, 1 T'-MoTe₂ films were obtained. Temperature, pressure, precursor amount, substrate, and gas flow are some important parameters in CVD synthesis. However, temperature plays a crucial role in CVD synthesis. It can affect not only the chemical reactions of precursors in the gas phase, the deposition rate of products on the substrate, and the flow of the carrier gas but also the strain on the growing material due to the difference in the thermal expansivity of the material, MoTe₂ and substrate, SiO₂/Si in our case. A previous report has demonstrated that the 1 T'-MoTe₂ phase grown by tellurization of a Mo thin film under a strain was converted into the 2H-MoTe₂ film by releasing the strain via the adoption of a prolonged growth time under Te atmosphere [12].

TST [33] can be applied to understand the strain-mediated phase stabilization of 2H-MoTe₂ and 1 T'-MoTe₂ at a lower temperature of 650 °C and a higher temperature of 730

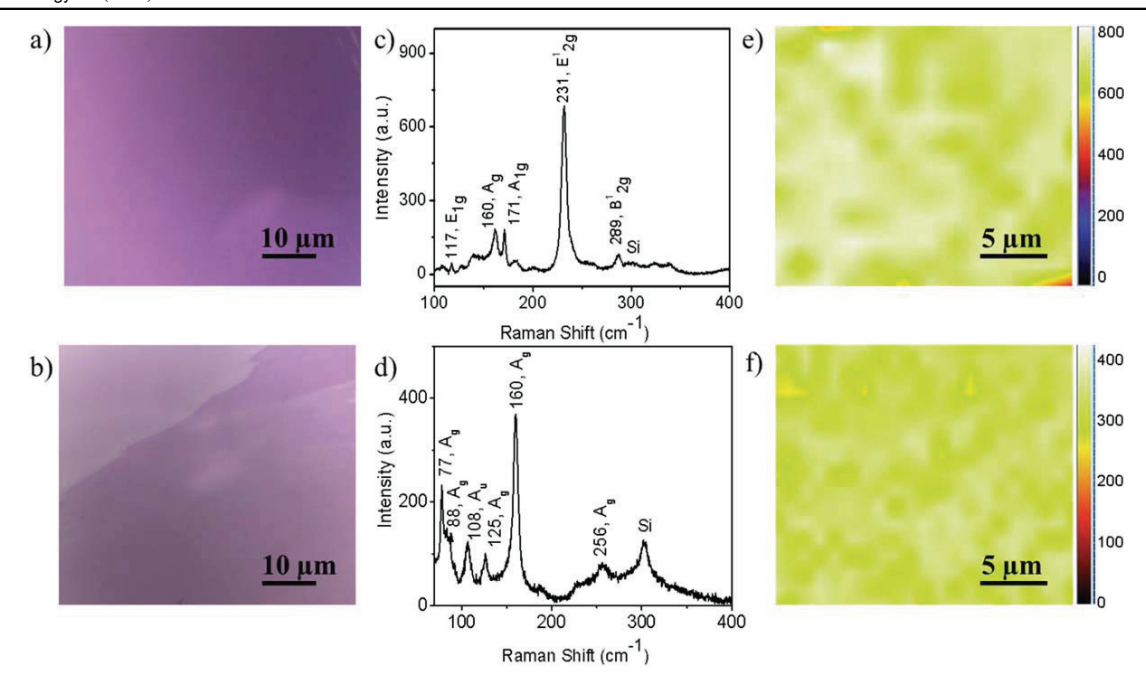


Figure 2. Optical images of (a) 2H-MoTe₂ phase, (b) 1 T'-MoTe₂ phase, Raman spectra collected with 532 nm laser excitation (c) 2H-MoTe₂ phase, (d) 1 T'-MoTe₂ phase and 22 μ m \times 20 μ m Raman maps for E_{2g}^1 peak intensity of (e) 2H-MoTe₂ phase, and Raman maps for A_g (f) 1 T'-MoTe₂ phase.

°C, respectively. According to TST, the stress/strain-dependent phase transition rate is given by $k(\sigma) \propto e^{-E_{\sigma}/k_BT}$, where k is the transition rate when a stress σ is applied, E_{σ} is the phase transition barrier energy, k_B is the Boltzmann constant, and T is the absolute temperature. Under zero or low stress/ strain condition at a lower growth temperature (e.g. 650 °C), 2H-MoTe₂ phase is more stable than 1 T'-MoTe₂, whereas the higher and sufficiently large stress/strain exerted on the growing material at a higher growth temperature (e.g. 730 °C) lowers the barrier energy (E_{σ}) , thereby making the 1 T'-MoTe₂ phase more thermodynamically favorable [8]. Hence, the growth and stabilization of 1 T'-MoTe₂ film at a higher temperature, 730 °C in our experiment could be attributed to the higher strain experienced by the growing material, and the growth and stabilization of 2H-MoTe₂ film at a lower temperature, 650 °C could be attributed to the lower strain on the growing material. The effect of strain on the phase change behavior of MoTe2 has also been demonstrated by Song et al [34] where the phase change from 2H- to 1 T'-MoTe₂ by the application of strain and reverse phase transition under removal of the strain, and reduction of the 2H- to 1 T'- phase transition temperature under a tensile strain have been demonstrated.

Figures 2(a) and (b) show optical images of 2H- and 1 T'-MoTe₂ films and figures 2(c) and (d) their corresponding Raman spectra. 2H-MoTe₂ exhibits Raman peaks at 117, 171, 231, and 289 cm⁻¹, which could be assigned to Raman active vibrational modes of E_{1g} , A_{1g} , E_{2g}^1 , and B_{2g}^1 , respectively [35, 36] (figure 2(c)). A prominent peak B_{2g}^1 appearing at 289 cm⁻¹indicates that the film contains few layers of MoTe₂ and the ratio of B_{2g}^1 to E_{2g}^1 is ~0.15, which corresponds to 6–7 layers of MoTe₂ [35]. The Raman peaks appearing with low

intensity at $\sim 160~\rm cm^{-1}$ correspond to $A_{\rm g}$ vibrational modes of 1 T'-phase, indicating the presence of a small amount of 1 T'-phase mixed in the 2H-MoTe₂ [35–37]. The formation of the 1 T'-MoTe₂ film is confirmed by the appearance of several Raman peaks at 77, 88 108, 125, 160, 256 cm⁻¹, among which the peak appearing at $108~\rm cm^{-1}$ is associated with the Raman active $A_{\rm u}$ vibrational mode, and all other peaks are associated with the Raman active $A_{\rm g}$ vibrational modes (figure 2(d)) [38–40].

Raman spectroscopy mappings over an area of 22 μ m \times $20 \,\mu\text{m}$ (440 points) for E_{2g}^1 peak (231 cm⁻¹) intensity of 2H-MoTe₂ film (figure 2(e)) and A_g peak (160 cm⁻¹) intensity of 1 T'-MoTe₂ film (figure 2(f)) were collected to ascertain the homogeneity of the synthesized films [37]. The black to whitish-green color in the scale bar of the Raman maps represents an increase in the intensity of the selected peaks. A small variation in the peak intensity from 600 to 800 cm⁻¹ as indicated by the green to whitish-green and the absence of black and blue color in the mapping image for 2H-MoTe₂ film indicate that the film is comprised of mainly 2H- phase. This can further be evidenced by the presence of a negligibly small number of the 1 T'-MoTe2 Raman spectra over the 440 points in the mapping area (see figure S1(a) (available online at stacks.iop.org/NANO/32/335701/mmedia) in the supporting file). Figure 2(f) also shows that almost 100% of the mapping area is green to whitish-green and there is no black or red color, indicating the presence of only 1 T'- phase and absence of 2H- phase. This result is further supported by the absence of the Raman spectra of the 2H-MoTe2 phase over the 440 points in the mapping area (see figure S1(b) in the supporting file).

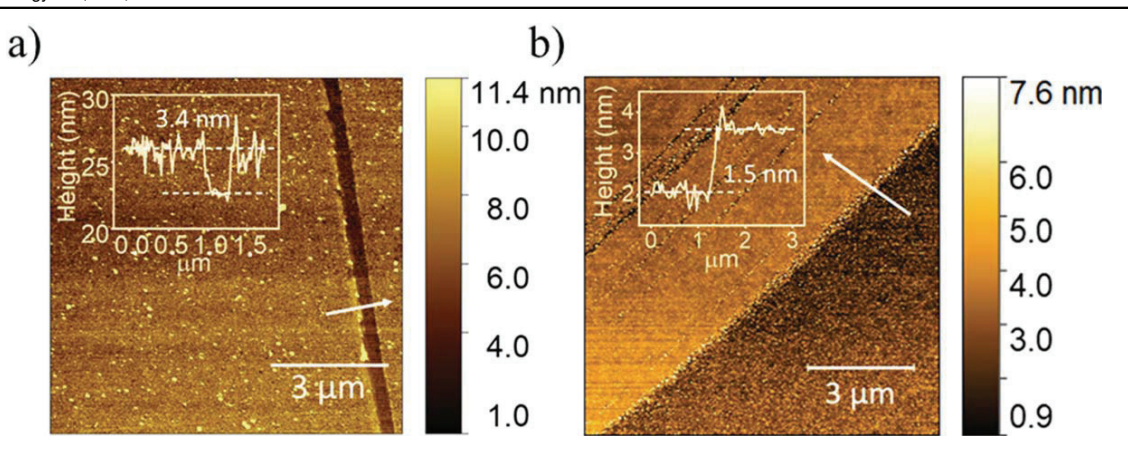


Figure 3. AFM images, height profile, and thickness of 2D MoTe₂ films using tapping mode (a) 2H- phase (b) 1 T'- phase.

The thickness and roughness of 2D MoTe₂ films were measured by AFM. Tapping mode AFM measurements indicate that the thickness of the 2H-MoTe₂ film (figure 3(a)) is \sim 3.4 nm, which is equivalent to \sim 6 layers of 2D MoTe₂. The AFM height profile of 1 T'-MoTe₂ film (figure 3(b)) shows a thickness of 1.5 nm corresponding to 2 layers of 2D MoTe₂. The root mean square (rms) roughness of 2H- and 1 T'-MoTe₂ films were measured as \sim 7 Å and \sim 3 Å for 2H- and 1 T'-MoTe₂, respectively.

3.2. SERS study

Two different sets of SERS experiments were performed using 2H- and 1 T'-MoTe₂ films. Figures 4(a) and (b) show SERS spectra of a solution of MB at different concentrations (from bottom to top: 3.1×10^{-5} , 3.1×10^{-6} , 3.1×10^{-7} , and 3.1×10^{-8} M) on 2H-MoTe₂ films using 532 nm and 633 nm laser excitations, respectively. Figures 4(c) and (d) show SERS spectra of various MB solution concentrations on 1 T'-MoTe₂ films by using laser excitation at 532 nm and 633 nm, respectively. SERS data show that Raman enhancement varies for two different polymorphs of MoTe₂ films. The Raman EF as calculated using the formula shown below, based on the intensity of an intense Raman peak occurring at 1620 cm⁻¹, which arises due to in-plane C–C stretching of the aromatic ring of MB [27, 41, 42].

$$EF = \frac{I_{SERS} / C_{SERS}}{I_{dense} / C_{dense}}, \tag{1}$$

where $I_{\rm SERS}$ is the Raman intensity at 1620 cm⁻¹ with a concentration of $C_{\rm SERS}$ and $I_{\rm dense}$ is the intensity of MB on the SERS inactive substrate, i.e. ${\rm SiO_2/Si}$, $C_{\rm dense}=1\,{\rm M}$. We obtained EF values for MB as 5.4×10^6 and 3.5×10^7 using 2H-MoTe₂ film, and 1.4×10^7 and 1.1×10^8 using 1 T'-MoTe₂ films with laser excitation at 532 nm and 633 nm, respectively.

The obtained Raman EF values have been compared with those of the CVD-grown TMDs reported previously in table 1. Our Raman EF obtained using 1 T'-MoTe₂ film is comparable to that reported by Tao *et al* [25] for CVD-synthesized 1 T'-MoTe₂ film and much higher than those

reported by others [24, 25, 43–46] for CVD-synthesized TMDs. Furthermore, the LOD as low as 10 nM for MB was achieved on both 2H- and 1 T'-MoTe₂ films, which is comparable to the most sensitive CVD-synthesized TMDs-based SERS substrates as presented in table 1. To the best of our knowledge, this is the first time that SERS activity of 2H-MoTe₂ film has been reported, and the result shows that semiconducting 2H-MoTe₂ film could serve as an efficient SERS substrate.

3.3. Raman enhancement mechanism

SERS substrates can enhance the Raman scattering of probe molecules in two ways: CM [48] and EM [18]. Both 2H-MoTe₂ and 1 T'-MoTe₂ have unique electronic properties which play key roles on the CM-based SERS mechanism, a first layer effect [41], where electronic coupling between probe molecules and the metal complex is responsible for SERS enhancement [25]. Raman enhancement phenomena can be explained by the unified theory of SERS as proposed by Lombardi and Birke [48]. According to the literature reported before [25, 27, 35], the Raman signal enhancement on 2D materials could mainly be due to CM via a CT process.

The Raman enhancement mechanism and the effect of molecular resonance transition on the MB-2D MoTe₂ system can be explained by an energy level diagram (figure 5).

There are mainly three resonance transitions involved in the MB-2D MoTe₂ system. The first transition responsible for SERS enhancement is a molecular transition ($\mu_{\rm mol}$) from the HOMO ($-6.26\,{\rm eV}$) to the LUMO ($-4.55\,{\rm eV}$) of MB molecule [49]. The excitation of MB molecules with laser energy matching the HOMO-LUMO energy difference, 1.71 eV (\sim 725 nm) causes a molecular resonance, contributing to a strong enhancement of the Raman signal. The second is CT transition ($\mu_{\rm i-CT}$) from the molecular HOMO to the Fermi level ($-4.59\,{\rm eV}$)[25] and CB ($-4.11\,{\rm eV}$) [50] of 1 T'- and 2H- phases respectively, which is also known as 'B' term in the Herzberg-Teller picture [51]. The third is the CT transition ($\mu_{\rm k-CT}$ or $h_{\rm ik}$) from the Fermi level to the CB of 2D MoTe₂ to the molecular LUMO. In the case of 2H-MoTe₂, there are

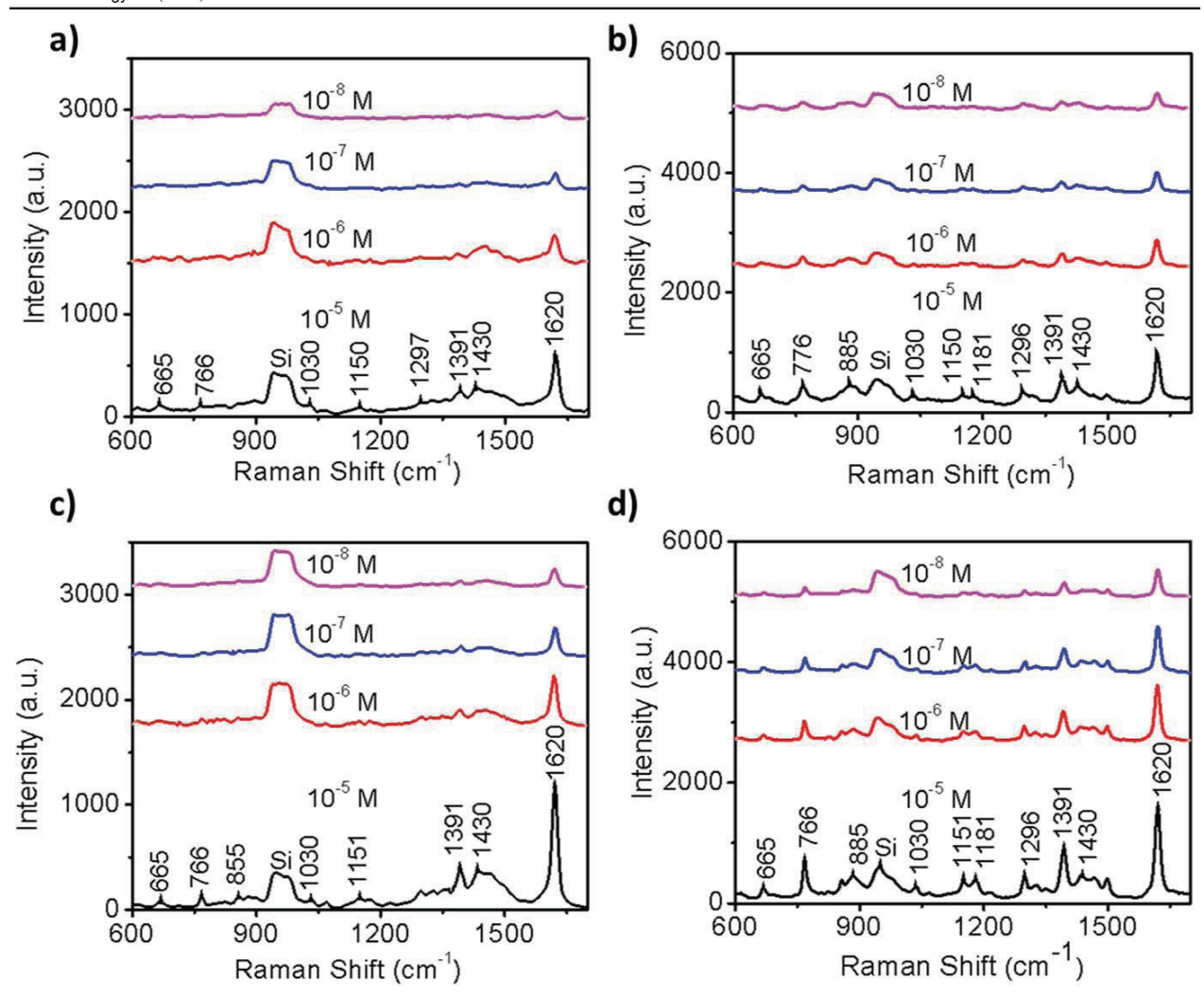


Figure 4. Top: SERS spectra of MB at different concentrations on 2H-MoTe₂ films measured under laser excitation at (a) 532 nm, and (b) 633 nm. Bottom: SERS spectra of MB at different concentrations on 1 T'-MoTe₂ films measured under laser excitation at (c) 532 nm, and (d) 633 nm.

additional two transitions that could occur i.e. a surface state that may be present in the bandgap (not shown here) to molecule LUMO and the VB of 2D MoTe₂ to molecule LUMO [22]. However, the energy of these two transitions is much smaller (less than 0.93 eV in the case of 2H-MoTe₂) than 532 and 633 nm laser photons, and hence the effect of these two transitions for excitation laser-dependent Raman enhancement can be neglected. The relatively larger Raman enhancement on 1 T'-MoTe₂ than 2H-MoTe₂ films and the laser wavelength-dependent Raman EF can be explained qualitatively by using the unified theory for SERS proposed by Lombardi and Birke [48], according to which a dominant 'B' term contributing to the Raman signal in SERS can be written as:

where $\langle i|Q_k|k\rangle$ is the vibration selection; ε_0 the permittivity of the surrounding medium(real part), ε_1 and ε_2 (real and imaginary) the permittivity of the SERS substrate (2H- and 1 T'-MoTe₂); ω is the laser frequency; ω_{i-CT} is the charge-transfer frequency; and γ_{i-CT} and γ_{mol} are the damping factors associated with the respective processes.

As stated before, CM is the dominant effect for the Raman enhancement in 2D MoTe₂, so plasmon excitation with both lasers has a negligible effect, and the first term in the denominator of equation (2) is not considered in our explanation. As a result, the second and third factors in the denominator of equation (2) associated with the charger transfer transition and molecular transition, respectively, are responsible for the Raman EF on 2D MoTe₂. When the

$$R_{iFk} = \frac{\mu_{i-CT} \mu_{mol} h_{ik} \langle i|Q_k|k\rangle}{((\varepsilon_1(\omega) + 2\epsilon_0)^2 + \varepsilon_2^2)(\omega_{i-CT}^2 - \omega^2 + \gamma_{i-CT}^2)(\omega_{mol}^2 - \omega^2 + \gamma_{mol}^2)},$$
(2)

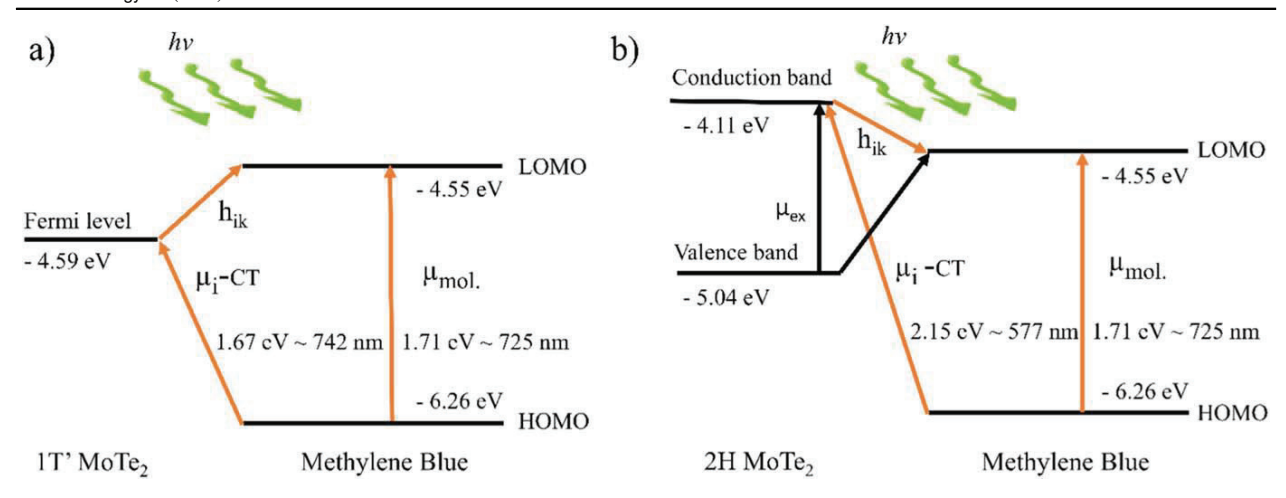


Figure 5. Energy level diagram showing CT process between 2D MoTe₂ films and MB molecule. (a) 1 T'- phase, and (b) 2H- phase.

Materials	Probe molecule	LOD	EF values	Laser (nm)	References
1 T'-MoTe	MB	10 nM	5.4×10^{8}	633	This work
2H-MoTe,	MB	10 nM	1.8×10^{7}	633	This work
1 T'-WTe	Rhodamine 6 G	40 fM	1.8×10^{9}	532	[25]
1 T'-MoTe,	Rhodamine 6 G	$0.4\mathrm{nM}$	$1.6 \times 10^{^{8}}$	532	[25]
1 T'-MoTe	β -Sitosterol	1 nM	1.0×10^{4}	785	[24]
1 T'-MoS,	MB	$1 \mu M$	6.0×10^{2}	633	[43]
2H-MoS	MB	10 mM	2.0×10^{2}	633	[43]
MoSSe	Glucose	$10 \mathrm{mM}$	1×10^{5}	532	[44]
2H-MoSe	4-Mercaptopyridine	1 nM	$3.5 \times 10^{\circ}$	488	[47]
WSe,	Cu-Phthalocyanine	N/A	3	632	[46]

Table 1. Raman EF comparison of different CVD-grown TMDs.

MB-1T'-MoTe₂ system is excited with 532 (2.33 eV) and 633 nm (1.96 eV) laser separately, the laser energy is enough to excite the electrons from HOMO to the Fermi level (6.26 –4.59 = 1.67 eV) as well as from molecular HOMO to LUMO (6.26 - 4.55 = 1.71 eV). However, the 633 nm laser energy is closer to both energy values associated with CT ($E_{i-\text{CT}} = 1.67 \, \text{eV}$) and molecular transitions ($E_{\text{mol}} = 1.71 \, \text{eV}$) as compared to 532 nm (2.33 eV) laser excitation (figure 5(a)), i.e. $\omega_{i-CT} \sim \omega$, and $\omega_{\text{mol}} \sim \omega$ for 633 nm. Hence, the Raman EF on MB-1T'-MoTe₂ system with 633 nm (1.1 × 10⁸) is significantly (~8-fold) higher than that of 532 nm (1.4 × 10⁷).

In the case of the MB-2H-MoTe₂ system (see figure 5(b)), the energies associated with CT transition and the molecular transition are $E_{i-\text{CT}}=6.26-4.11=2.15\,\text{eV}$ (\sim 577 nm) and $E_{\text{mol}}=1.71\,\text{eV}$ (\sim 725 nm), respectively. We observed that 633 nm laser excitation is closer to both of $E_{\text{mol}}=1.71\,\text{eV}$, but both 532 and 633 nm laser energies are equally close to $E_{i-\text{CT}}=2.15\,\text{eV}$ (\sim 577 nm). Hence, the overall observed Raman EF with 633 nm laser excitation is about 6-fold higher than that observed with 532 nm can be explained with the presented energy diagram. Our results clearly illustrate that the 1 T'-MoTe₂ film is more efficient than the 2H-MoTe₂ film for SERS enhancement. The higher Raman EF observed on 1 T'-MoTe₂ films as compared to that

observed on 2H-MoTe₂ films could be attributed to the higher electronic density of states near the Fermi level in 1 T'-MoTe2, which facilitates CT transition thereby enhancing the molecular polarizability of MB molecule. Nonetheless, the surface defects of the films could magnify the SERS enhancement via a combined effect of increased charge density and PICT pathways [52]. It is well understood that the FWHM of the Raman peaks increases with the increase in defect density in a material, and a material having a significant number of defects shows a broad Raman peak [53, 54]. In our case, both 2H- and 1 T'-MoTe₂ films show high crystallinity as indicated by the sharp Raman peaks with FWHM \sim 5.1 cm⁻¹ of E_{2g}^1 peak for 2H- film and \sim 4.9 cm⁻¹ of Ag peak for 1 T'-MoTe2 film, which are comparable to those of highly crystalline mechanically exfoliated singlecrystal 2D MoTe₂ in the reports [50, 55, 56]. As a result, the defects in the films should not significantly modulate the SERS performance, and the higher SERS performance (significantly large EF \sim 3 times) of the 1 T'-MoTe₂ film is due to the intrinsic property of the material. Our results also showed that Raman enhancement by CM is strongly dependent on the energy of laser excitation, analytes, and SERS substrate, which is in an excellent agreement with previous reports [27, 47, 50].

4. Conclusion

We presented a facile approach for the phase-controlled synthesis of 2H- and 1 T'-MoTe₂ films directly on SiO₂/Si substrates via APCVD. The SERS properties of as-grown 2D MoTe₂ were evaluated with MB, using Raman spectroscopy. The results showed that the Raman EF ($\sim 10^7 - 10^8$) on 1 T'-MoTe₂ was 3 times higher than that on 2H- MoTe₂, which could be explained by the fact that higher electronic density of states near the Fermi level is semi-metallic 1 T'-MoTe₂ facilitates photon-induced charge-transfer interaction. The higher Raman EF obtained with 633 nm laser excitation versus 532 nm could be attributed to charger transfer transitions and molecular transitions between MB and the substrate. The realization of a LOD of ~10 nM MB molecules suggests that CVD-grown 1 T'-MoTe2 film could serve as a promising flat platform for SERS-based chemical sensing.

Acknowledgments

The authors are grateful for the financial support of this project by the US National Science Foundation (Awards # 1831133 and #1523617). The authors thank Dr. Basant Chitara and Mr. Thakur Sapkota for their technical assistance in the synthesis and characterization of 2D MoTe₂.

Data availability statement

All data that support the findings of this study are included within the article (and any supplementary files).

ORCID iDs

Fei Yan https://orcid.org/0000-0001-5983-143X

References

- Novoselov K S et al 2004 Electric field effect in atomically thin carbon films Science 306 666–9
- [2] Chauhan J and Guo J 2011 Assessment of high-frequency performance limits of graphene field-effect transistors *Nano Res.* 4 571–9
- [3] Wang Z et al 2016 Electrostatically tunable lateral MoTe₂ p-n junction for use in high-performance optoelectronics Nanoscale 8 13245–50
- [4] Seok J et al 2017 Active hydrogen evolution through lattice distortion in metallic MoTe₂ 2D Mater. 4 025061
- [5] Lv R et al 2015 Transition metal dichalcogenides and beyond: synthesis, properties, and applications of single- and fewlayer nanosheets Acc. Chem. Res. 48 56–64
- [6] Wang Y et al 2017 Structural phase transition in monolayer MoTe₂ driven by electrostatic doping Nature 550 487–91
- [7] Empante T A et al 2017 Chemical vapor deposition growth of few-layer MoTe₂ in the 2H, 1T', and 1T phases: tunable properties of MoTe₂ films ACS Nano 11 900-5

- [8] Keum D H et al 2015 Bandgap opening in few-layered monoclinic MoTe₂ Nat. Phys. 11 482–6
- [9] Pradhan N R et al 2014 Field-effect transistors based on fewlayered α-MoTe₂ ACS Nano 8 5911–20
- [10] Nakaharai S, Yamamoto M, Ueno K and Tsukagoshi K 2016 Carrier polarity control in α-MoTe₂ Schottky junctions based on weak Fermi-level pinning ACS Appl. Mater. Interfaces 8 14732–9
- [11] Cho S *et al* 2015 Phase patterning for ohmic homojunction contact in MoTe₂ *Science* **349** 625–8
- [12] Park J C et al 2015 Phase-engineered synthesis of centimeterscale 1T'- and 2H-molybdenum ditelluride thin films ACS Nano 9 6548–54
- [13] Zhou J et al 2017 Large-area and high-quality 2D transition metal telluride Adv. Mater. 29 1603471
- [14] Zhou L et al 2015 Large-area synthesis of high-quality uniform few-layer MoTe₂ J. Am. Chem. Soc. 137 11892–5
- [15] Grubisha D S, Lipert R J, Park H-Y, Driskell J and Porter M D 2003 Femtomolar detection of prostate-specific antigen: an immunoassay based on surface-enhanced Raman scattering and immunogold labels *Anal. Chem.* 75 5936–43
- [16] Schlücker S 2014 Surface-enhanced Raman spectroscopy: concepts and chemical applications Angew. Chemie Int. Ed. 53 4756–95
- [17] Schlücker S 2010 Surface-Enhanced Raman spectroscopy: Analytical, Biophysical and Life Science Applications (Weinheim, Germany: Wiley-VCH Verlag GmbH & Co. KGaA)
- [18] Ding S, Moskovits M and You E 2017 Electromagnetic theories of surface-enhanced Raman spectroscopy *Chem. Soc. Rev.* 46 4042–76
- [19] Lee Y et al 2016 Enhanced Raman scattering of Rhodamine 6G films on two-dimensional transition metal dichalcogenides correlated to photoinduced charge transfer Chem. Mater. 28 180–7
- [20] Zheng T, Zhou Y, Feng E and Tian Y 2021 Surface-enhanced Raman scattering on 2D nanomaterials: recent developments and applications *Chin. J. Chem.* 39 745–56
- [21] Orlando D J, Kahn E, Wong Y C, Yeh Y T, Limbu T B, Chitara B, Elias L, Terrones M and Yan F 2019 Ultrastrong Raman- enhancement on gold nanoparticle-decorated transition metal dichalcogenides nanosheets for molecule detection J. Anal. Sci. 35 1–6
- [22] Han X X, Ji W, Zhao B and Ozaki Y 2017 Semiconductorenhanced Raman scattering: active nanomaterials and applications *Nanoscale* 9 4847–61
- [23] Fraser J P et al 2020 Selective phase growth and precise-layer control in MoTe₂ Commun. Mater. 1 48
- [24] Fraser J P et al 2020 Application of a 2D molybdenum telluride in SERS detection of biorelevant molecules ACS Appl. Mater. Interfaces 12 47774–83
- [25] Tao L et al 2018 1T' Transition metal telluride atomic layers for plasmon-free SERS at femtomolar levels J. Am. Chem. Soc. 140 8696–704
- [26] Kitadai H, Wang X, Mao N, Huang S and Ling X 2019 Enhanced Raman scattering on nine 2D van der Waals materials J. Phys. Chem. Lett. 10 3043–50
- [27] Limbu T B et al 2020 Unravelling the thickness dependence and mechanism of surface-enhanced Raman scattering on Ti₃C₂T_X MXene nanosheets J. Phys. Chem. C 124 17772–82
- [28] Yao J D, Zheng Z Q and Yang G W 2019 Production of largearea 2D materials for high-performance photodetectors by pulsed-laser deposition *Prog. Mater. Sci.* 106 100573
- [29] Vishwanath S et al 2015 Comprehensive structural and optical characterization of MBE grown MoSe₂ on graphite, CaF₂, and graphene 2D Mater. 2 024007
- [30] Kim T W et al 2018 Wafer-scale epitaxial 1T', 1T'-2H mixed, and 2H phases MoTe₂ thin films grown by metal-organic chemical vapor deposition Adv. Mater. Interfaces 5 1-8

- [31] Xu X et al 2019 Millimeter-scale single-crystalline semiconducting MoTe₂ via solid-to-solid phase transformation J. Am. Chem. Soc. 141 2128–34
- [32] He T et al 2019 Synthesis of large-area uniform MoS₂ films by substrate-moving atmospheric pressure chemical vapor deposition from monolayer to multilayer 2D Mater. 6 025030
- [33] Ghasemi A and Gao W 2020 Atomistic mechanism of stress modulated phase transition in monolayer MoTe₂ Extrem Mech. Lett. 40 100946
- [34] Song S, Keum D H, Cho S, Perello D, Kim Y and Lee Y H 2016 Room temperature semiconductor-metal transition of MoTe₂ thin films engineered by strain *Nano Lett.* 16 188–93
- [35] Yamamoto M et al 2014 Strong enhancement of Raman scattering from a bulk-inactive vibrational mode in few-layer MoTe₂ ACS Nano 8 3895–903
- [36] Predel B 1997 Mo-Te (Molybdenum-Tellurium) Li-Mg—Nd-Zr (Berlin, Heidelberg: Springer-Verlag)
- [37] Xu X et al 2020 Atomic-precision repair of a few-layer 2H-MoTe₂ thin film by phase transition and recrystallization induced by a heterophase interface Adv. Mater. 32 1–6
- [38] Beams R et al 2016 Characterization of few-layer 1T' MoTe₂ by polarization-resolved second harmonic generation and Raman scattering ACS Nano 10 9626–36
- [39] Zhang K et al 2016 Raman signatures of inversion symmetry breaking and structural phase transition in type-II Weyl semimetal MoTe₂ Nat. Commun. 7 1–6
- [40] Zhu M et al 2019 Linear dichroism and nondestructive crystalline identification of anisotropic semimetal few-layer MoTe₂ Small 1903159 1–8
- [41] Naujok R R, Duevel R V and Corn R M 1993 Fluorescence and Fourier transform surface-enhanced Raman scattering measurements of methylene blue adsorbed onto a sulfurmodified gold electrode *Langmuir* 9 1771–4
- [42] Limbu T B et al 2020 Green synthesis of reduced Ti₃C₂T_X MXene nanosheets with enhanced conductivity, oxidation stability, and SERS activity J. Mater. Chem. C 8 4722–31
- [43] Song X *et al* 2019 Plasmon-free surface-enhanced Raman spectroscopy using metallic 2D materials *ACS Nano* 13

- [44] Jia S et al 2020 Biomolecule sensing by surface-enhanced Raman scattering of monolayer Janus transition metal dichalcogenide Nanoscale 12 10723–9
- [45] Muehlethaler C, Considine C R, Menon V, Lin W C, Lee Y H and Lombardi J R 2016 Ultrahigh Raman enhancement on monolayer MoS₂ ACS Photon. 3 1164–9
- [46] Liu Y, Gao Z, Chen M, Tan Y and Chen F 2018 Enhanced Raman scattering of CuPc films on imperfect WSe₂ monolayer correlated to exciton and charge-transfer resonances Adv. Funct. Mater. 28 1805710
- [47] Lombardi J R and Birke R L 2009 A unified view of surfaceenhanced Raman scattering Acc. Chem. Res. 42 734–42
- [48] Shen J S, Yu T, Xie J W and Jiang Y B 2009 Photoluminescence of CdTe nanocrystals modulated by methylene blue and DNA A label-free luminescent signaling nanohybrid platform *Phys. Chem. Chem. Phys.* 11 5062–9
- [49] Rasmussen F A and Thygesen K S 2015 Computational 2D materials database: electronic structure of transition-metal dichalcogenides and oxides J. Phys. Chem. C 119 13169–83
- [50] Lombardi J R and Birke R L 2014 Theory of surface-enhanced Raman scattering in semiconductors J. Phys. Chem. C 118 11120–30
- [51] Song G, Gong W, Cong S and Zhao Z 2021 Ultrathin twodimensional nanostructures: surface defects for morphologydriven enhanced semiconductor SERS Angew. Chem. - Int. Ed. 60 5505–11
- [52] Pollard A J 2016 Metrology for graphene and 2D materials Meas. Sci. Technol. 27 09200157
- [53] Lin C-P et al 2019 Local modulation of electrical transport in 2D layered materials induced by electron beam irradiation ACS Appl. Electron. Mater. 1 684–91
- [54] Ji H et al 2017 Tunable mobility in double-gated MoTe₂ field-effect transistor: effect of Coulomb screening and trap sites ACS Appl. Mater. Interfaces 9 29185–92
- [55] Wang M, Li D, Liu K, Guo Q, Wang S and Li X 2020 Nonlinear optical imaging, precise layer thinning, and phase engineering in MoTe₂ with femtosecond laser ACS Nano 14 11169–77
- [56] Ghosh B, Saha P and Mukherjee G D 2020 Anomalous compressibility in 1T' MoTe₂ single crystal: high-pressure Raman and structural studies 1–15 arXiv:2001.01489[cond-mat.mtrl-sci]